Clinical Implant Dentistry and Related Research / Volume 27, Issue 1 / e70000

ORIGINAL ARTICLE | Open Access

Artificial Intelligence-Based Detection and Numbering of Dental Implants on Panoramic Radiographs

Yunus Balel, Kaan Sağtaş, Fatih Teke, Mehmet Ali Kurt

First published: 23 January 2025

https://doi.org/10.1111/cid.70000

Funding: The authors received no specific funding for this work.

ABSTRACT

Objectives

This study aimed to develop an artificial intelligence (AI)-based deep learning model for the detection and numbering of dental implants in panoramic radiographs. The novelty of this model lies in its ability to both detect and number implants, offering improvements in clinical decision support for dental implantology.

Materials and Methods

A retrospective dataset of 32 585 panoramic radiographs, collected from patients at Sivas Cumhuriyet University between 2014 and 2024, was utilized. Two deep-learning models were trained using the YOLOv8 algorithm. The first model classified the regions of the jaw to number the teeth and identify implant regions, while the second model performed implant segmentation. Performance metrics including precision, recall, and F1-score were used to evaluate the model's effectiveness.

Results

Back

recall from 0.895 to 0.956, and F1-scores from 0.917 to 0.966 across various jaw regions. The analysis revealed that implants were most frequently located in the maxillary posterior region.

Conclusions

The AI model demonstrated high accuracy in detecting and numbering dental implants in panoramic radiographs. This technology offers the potential to reduce clinicians' workload and improve diagnostic accuracy in dental implantology. Further validation across more diverse datasets is recommended to enhance its clinical applicability.

Clinical Relevance

This AI model could revolutionize dental implant detection and classification, providing fast, objective analyses to support clinical decision-making in dental practices.

1 Introduction

Panoramic radiographs are one of the most commonly used types of radiography in dentistry for visualizing teeth, jaws, and surrounding structures [1]. The interpretation of these images, which are used to provide diagnostic information, requires expertise and can be time-consuming. Manual analysis of these images using traditional methods is prone to human error and has limited efficiency, particularly when evaluating large datasets [2, 3].

Technological advancements in artificial intelligence (AI) have found applications in the medical field, just as in many other areas [4, 5]. The development of AI's capabilities in image analysis has enabled the automated processing and analysis of radiographic images [6-8]. Through deep learning algorithms, it has become possible to perform various diagnostic functions in dental radiographs, such as detecting dental caries, impacted teeth, and pathological formations [9-12]. These algorithms, trained on large datasets, can detect details that might be overlooked by the human eye, thereby reducing clinical error [13, 14].

Although there are algorithms in the literature that enable the detection of dental implants using AI, to the best of our knowledge, these algorithms have not addressed the numbering of dental implants [15, 16]. The use of AI-based systems for the detection and numbering of dental implants offers several potential benefits. First, these systems can quickly process large datasets, reducing the workload of dentists and saving time. Second, AI models offer objective evaluations, minimizing human errors [13]. Third, these technologies can produce more consistent and reliable results, especially in complex cases, thus improving the accuracy of clinical decisions.

Back

technology can be integrated into current clinical practices and explore the potential future applications of AI-based solutions in dentistry. It is expected that this study will make a significant contribution to existing approaches for the detection of dental implants in panoramic radiographs, offering improvements in clinical practice.

2 Materials and Methods

This retrospective study was approved by the Non-Interventional Clinical Research Ethics Committee of Sivas Cumhuriyet University with application number 24-07-38. The dataset consists of panoramic radiographs of patients who visited the Department of Oral and Maxillofacial Surgery at Sivas Cumhuriyet University, Faculty of Dentistry, between January 1, 2014, and July 1, 2024. In this study, conducted in accordance with the Helsinki Declaration, no written or verbal consent was obtained from the patients due to the retrospective nature of the anonymous data reviewed.

2.1 Dataset

A specific dataset was created for this study by labeling panoramic radiographs containing dental implants and natural teeth. Two experts, an oral and maxillofacial surgeon and a dentist, labeled the images using the Computer Vision Annotation Tool (CVAT, MIT License) installed on local computers. The labeling process was performed separately for tooth numbering and implant segmentation based on the FDI tooth numbering system, excluding third molars. During the data labeling process, the coronal parts of angled implants were annotated as the corresponding tooth number they aligned with. Since our dataset does not include zygomatic implants, the annotation of zygomatic implants was excluded from this study.

2.2 Data Augmentation Methods

In this study, various data augmentation techniques were applied to train the YOLOv8 model for detecting and segmenting dental implants in panoramic radiographs. Data augmentation aims to enhance the model's generalization ability and reduce overfitting by applying a set of transformations to a limited dataset. The methods used in this study are detailed below.

2.2.1 Geometric Transformations

To simulate various positions and orientations of the images, the following geometric operations were performed:

Horizontal Flip: Images were horizontally flipped to enable the model to recognize implants in symmetrical positions.

Shift and Scaling (Shift-Scale-Rotate): Random shifts (up to 5%) and scaling (up to 10%) were applied to augment the dataset with different positions of implants.

2.2.2 Brightness and Contrast Adjustments

To improve the model's performance under varying imaging conditions, the following operations were performed:

Brightness and contrast adjustment (random brightness contrast): Random changes in brightness and contrast were applied to the images.

CLAHE (contrast limited adaptive histogram equalization): This technique was used to enhance the contrast of the images.

2.2.3 Blur and Noise Addition

To simulate degraded image quality, the following operations were implemented:

Gaussian Blur: Images were blurred to improve the model's generalization performance for low-quality radiographs.

Noise Addition: Random noise was introduced to model environmental artifacts present in radiographs.

2.2.4 Augmentation Pipeline

The aforementioned operations were structured into a data augmentation pipeline. The *Albumentations* library was utilized to implement these augmentations, ensuring compatibility with annotation data. Segmentation masks and bounding box annotations were automatically updated after each augmentation. The pipeline was configured as follows:

2.2.5 Visualization of Results

To validate the correctness of the augmentations, the results were visualized using *matplotlib* and compared with the original images. This process ensured both the visual quality of the augmentations and their alignment with the annotations.

To ensure the robustness of the YOLOv8 model, a comprehensive data augmentation pipeline was employed. Techniques included geometric transformations (horizontal flipping, rotation, shift-scale-rotate) to simulate variations in implant positioning, as well as brightness/contrast adjustments and noise addition to mimic real-world imaging conditions. These augmentations, implemented using the Albumentations library, significantly improved model generalizability and reduced overfitting. The reason for applying these techniques was to ensure that nonstandardized panoramic radiographs could be evaluated correctly by the model. Examples of augmented images are provided in Figure S1.

Back

To improve model performance, two separate AI models were developed for tooth numbering and implant segmentation in dentistry. These models were created using the Ultralytics YOLOv8 algorithm, with enhancements for detection and segmentation tasks.

The detection model was developed using the object detection architecture of Ultralytics YOLOv8. This model takes radiographic images as input and detects the location of each tooth, assigning the appropriate FDI tooth number to each detected position. The YOLO architecture ensures fast and efficient detection, allowing accurate numbering of the teeth.

The segmentation model was created using the segmentation feature of Ultralytics YOLOv8. This model identifies and delineates the boundaries of the implant at the pixel level. The architecture is YOLO-based but equipped with a segmentation head, enabling precise masking of the implant region. Both models incorporate key layers such as convolutional neural networks (CNNs) and the grid-based detection method of YOLO, and the model architecture is schematized in Figure 1.

FIGURE 1

Open in figure viewer | PowerPoint

Model architecture.

Additionally, to evaluate the performance of the model across different architectures, Faster R-CNN, DETR (DEtection TRansformer), and RetinaNet architectures were used for the detection model, while U-Net, Mask R-CNN, and DeepLab (v3+) architectures were used for the segmentation model. However, since the highest results were obtained with the YOLOv8 detection and YOLOv8 segmentation architectures, it was decided to report only the results of the YOLOv8 architecture in this study. The training results obtained with the other architectures are provided in Table S1.

2.4 Model Training

Back

The main parameters used in the training of both models were as follows:

Image format and size: All images in jpg, png, gif, tif, and bmp formats were resized to 640 × 640 for training.

Learning rate: The initial learning rate was set to 0.001 and dynamically reduced during training.

Batch size: The batch size was set to 16.

Epoch count: Training continued for 100 epochs.

Loss and metric calculation: The mean average precision (mAP) metric was used for the tooth numbering model, while the Intersection over Union (IoU) metric was used for the implant segmentation model [17, 18]. Both models were trained using the stochastic gradient descent (SGD) optimization algorithm to minimize loss [19].

Model validation and evaluation: During training, performance was monitored using a validation set, and early stopping with a dropout rate of 20% between layers was applied to prevent overfitting. The best-performing weights were saved at the end of each epoch, and the weights achieving the highest score on the validation set were used for testing.

Training and testing were completed on a workstation with an Intel 12 900K processor, 128GB DDR5 RAM, and an Nvidia Quadro A6000 GPU.

2.5 Statistical Analysis

True positives (TP), True negatives (TN), False positives (FP), and False negatives (FNs) were used as foundational metrics to analyze the model's classification behavior, identifying correct and incorrect predictions. Precision, which measures the proportion of correctly identified positive cases among all predicted positives, was crucial to minimize FP and their potential clinical consequences. Recall (sensitivity) evaluated the model's ability to identify all TP, ensuring no implants were missed, as FN could significantly impact patient care. The F1 score, representing the harmonic mean of precision and recall, balanced these metrics to provide a holistic measure of the model's accuracy.

Precision =

F1 score =

Recall (sensitivity) =

Additionally, mAP50 (mean average precision at 50% IoU) quantified detection accuracy at a 50% overlap threshold, assessing the spatial precision of predictions.

Back

performance under varying spatial tolerances.

These metrics together provided a thorough evaluation framework, ensuring the model's reliability and effectiveness for clinical applications.

3 Results

A total of 32 585 panoramic radiographs from different patients were used in the training, validation, and test sets: 24 577 for training, 6195 for validation, and 1813 for testing. Of the patients, 54.92% (17986) were female, and 45.08% (14689) were male.

Twenty-eight different classes were created for numbering tooth-implant regions. In the test dataset, consisting of 1813 images. The confusion matrices showing the performance of the detection and segmentation models on the test set are presented in Figure 2. The results of the detection model indicate that the model can classify positive examples with quite high accuracy. The model identified 5772 examples as TP, while only classifying 201 examples as FP. In terms of negative examples, the model produced 538 TN and 201 incorrect FN (Figure 2A). The performance evaluation of the segmentation model demonstrates the model's capacity to successfully classify positive examples while revealing more difficulty in classifying negative examples. The segmentation model classified 5901 examples as TP but made 363 FP classifications. The number of TN examples was recorded as 58, while the FN count was 390 (Figure 2B). The precision, recall, F1 score, mAP50, and mAP50-90 values obtained for both models are presented in Table 1.

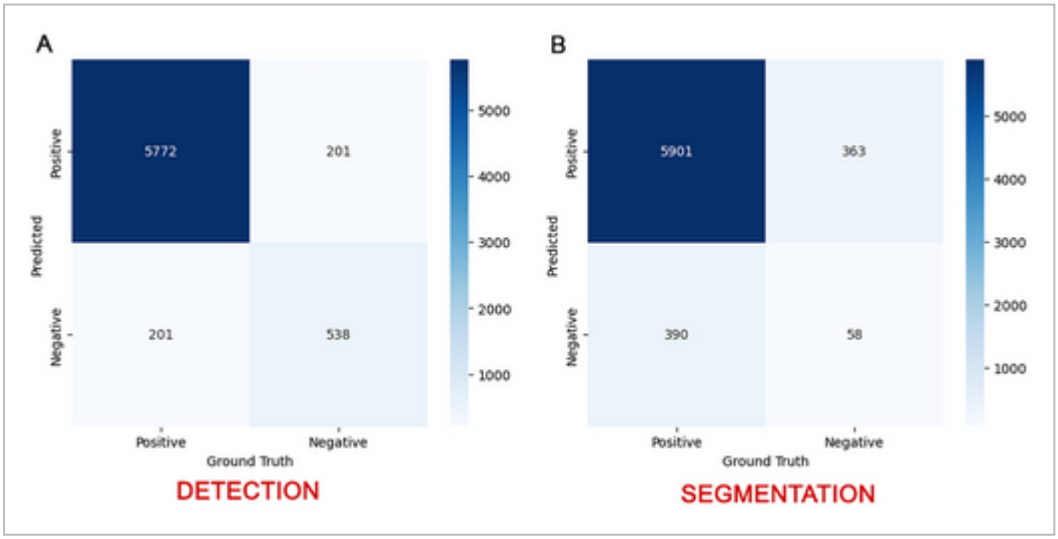

FIGURE 2

Open in figure viewer | PowerPoint

Confusion matrix results for detection and segmentation models.

Back

Implant numbering model (YOLOv8 detection)						
Class	**Number of images**	**Precision**	**Recall**	**F1**	**mAP50**	**mAP50-95**
11	1760	0.976	0.956	0.966	0.976	0.912
12	1739	0.971	0.949	0.960	0.972	0.885
13	1723	0.966	0.941	0.953	0.968	0.883
14	1750	0.965	0.899	0.931	0.946	0.848
15	1722	0.958	0.895	0.925	0.942	0.852
16	1735	0.952	0.918	0.935	0.954	0.877
17	1679	0.94	0.896	0.917	0.94	0.866
21	1780	0.979	0.945	0.962	0.971	0.911
22	1757	0.978	0.94	0.959	0.969	0.877
23	1728	0.971	0.934	0.952	0.965	0.881
24	1750	0.966	0.902	0.933	0.948	0.85
25	1722	0.959	0.903	0.930	0.947	0.854
26	1762	0.962	0.902	0.931	0.947	0.868
27	1716	0.95	0.898	0.923	0.943	0.871

Implant segmentation model (YOLOv8 Segmentation)						
Implant	1813	0.914	0.905	0.931	0.943	0.65

The implant segmentation model achieved a precision of 0.914, a recall of 0.905, and an F1 score of 0.931. The tooth-implant region numbering model had precision values ranging from 0.94 (lowest for tooth number 17) to 0.981 (highest for tooth number 33), recall values ranging from 0.895 (lowest for tooth number 15) to 0.956 (highest for tooth number 11), and F1 scores ranging from 0.917 (lowest for tooth number 17) to 0.966 (highest for tooth numbers 11 and 33).

To analyze the distribution of dental implants, a correlogram in Figure 3 was used. In this correlogram, “x” represents the horizontal position, “y” represents the vertical position,

Back

Darker images indicate denser labeling. The X–Y correlogram shows that implants are most commonly found in the maxillary posterior region, followed by the mandibular posterior, maxillary anterior, and mandibular anterior regions. The width histogram indicates that width values are low, with implant diameters generally concentrated between 0.0 and 0.1, suggesting that most implants fall within a specific diameter range. Scatterplots of width against x and y positions show a widespread distribution with no apparent correlation. The height histogram demonstrates that implant heights are generally low, concentrated between 0.0 and 0.05, indicating similar and relatively short implants. Scatterplots of height with other variables show no clear correlation between height and other factors.

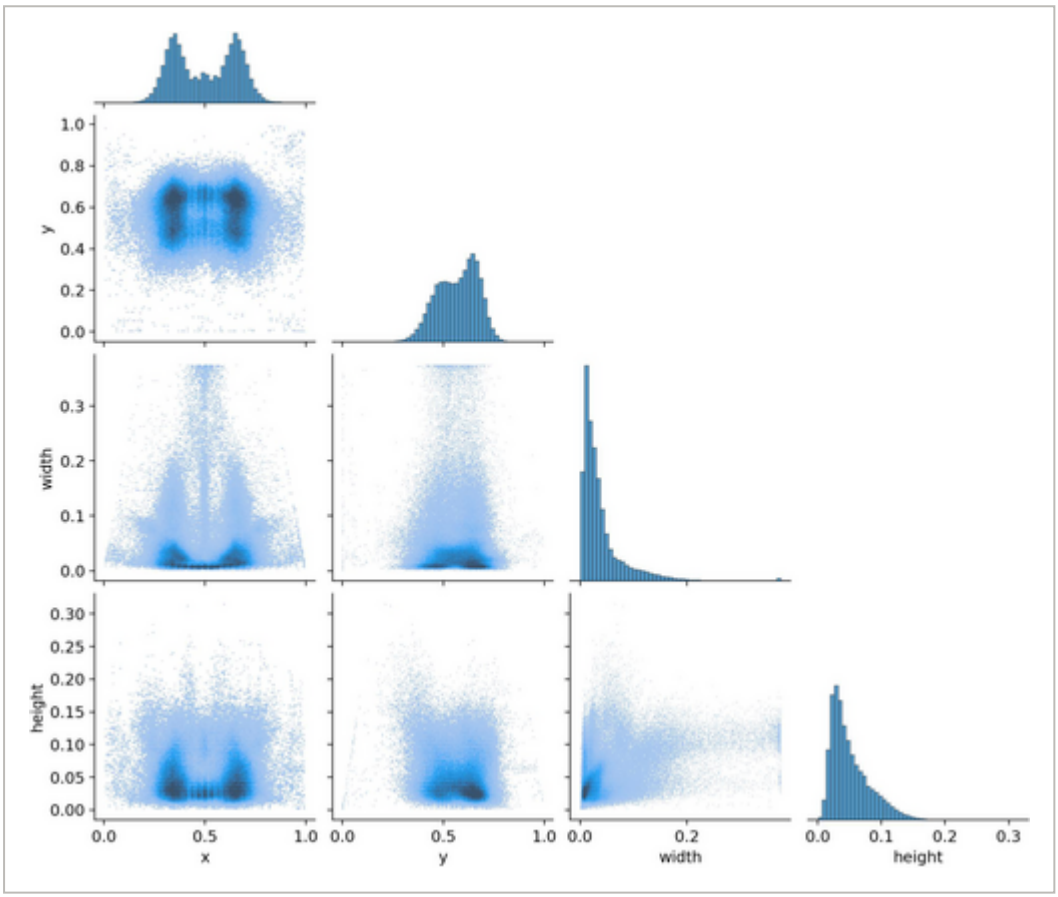

FIGURE 3

Open in figure viewer | PowerPoint

Correlogram of dental implant position and size distributions.

Figure 4 illustrates the training losses and performance metrics for the deep learning model during the training and validation phases. The graphs display separate loss and success metrics for box detection and classification tasks (segmentation and classification). The interpretation of this figure is as follows:

Back

better-bounding box positioning by the model.

train/seg_loss: Displays the segmentation loss. The initially high error decreases over time, improving the model's segmentation ability, though the curve has not fully flattened, indicating the model is still learning segmentation.

train/cls_loss: Represents classification loss. Initially high, the loss decreases over time, showing that the model becomes more accurate in classification.

train/dfl_loss: Represents the “distributional focal loss.” The rapid decrease in loss indicates quick improvement in this metric as well.

metrics/precision(B) and metrics/recall(B): These graphs show the model's performance for box detection in terms of precision and recall. Precision improves over time, with occasional fluctuations, reflecting an increase in the proportion of correctly detected positive examples. Recall improves rapidly from an initially low value, indicating the model's growing ability to detect positive examples.

metrics/precision(M) and metrics/recall(M): Represent the precision and recall values for the M task (segmentation/classification). Precision (M) improves over time, showing that the model becomes more stable and accurate in segmentation or classification. Recall (M) shows a rapid improvement from an initially low value.

metrics/mAP50(B) and metrics/mAP50-95(B): mAP50 (mean average precision at 50 IoU threshold) evaluates the model's overall accuracy in object detection. mAP50-95 measures the average accuracy across different IoU thresholds. mAP50 (B) improves rapidly and stabilizes, indicating high performance in box detection. mAP50-95 (B) shows improved performance across different IoU values, demonstrating broader success.

metrics/mAP50(M) and metrics/mAP50-95(M): Represent mAP values for segmentation or classification. Similar to mAP50(B), these metrics also show improvement over time, with initial low values rising quickly.

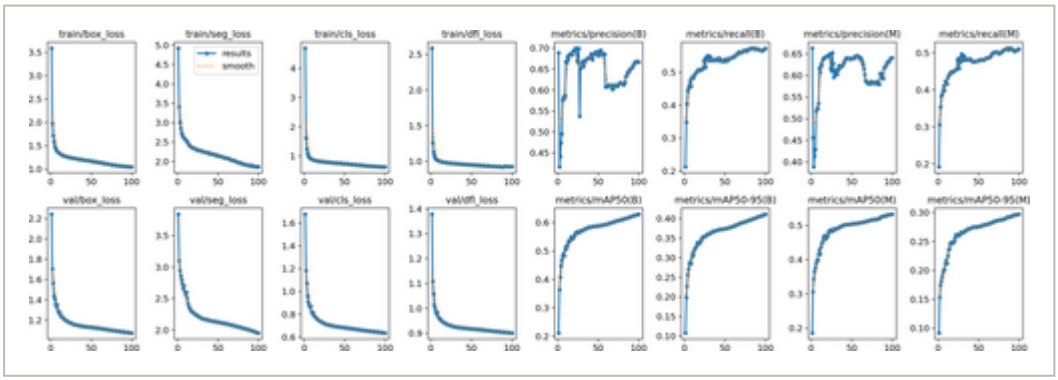

FIGURE 4

Back

Figure 5 shows how the F1 score changes against confidence levels for the developed deep learning model. This curve highlights a significant change in performance based on confidence levels. Notably, a marked drop in the F1 score occurs when the confidence exceeds 0.8, indicating that the model begins classifying only the most certain predictions as positive, increasing the risk of missing TP cases. Hence, the algorithm's optimal performance is observed within the 0.0 to 0.8 confidence range, where both high precision and high recall are achieved. This finding emphasizes the importance of using the model within this confidence range for accurate dental implant classification.

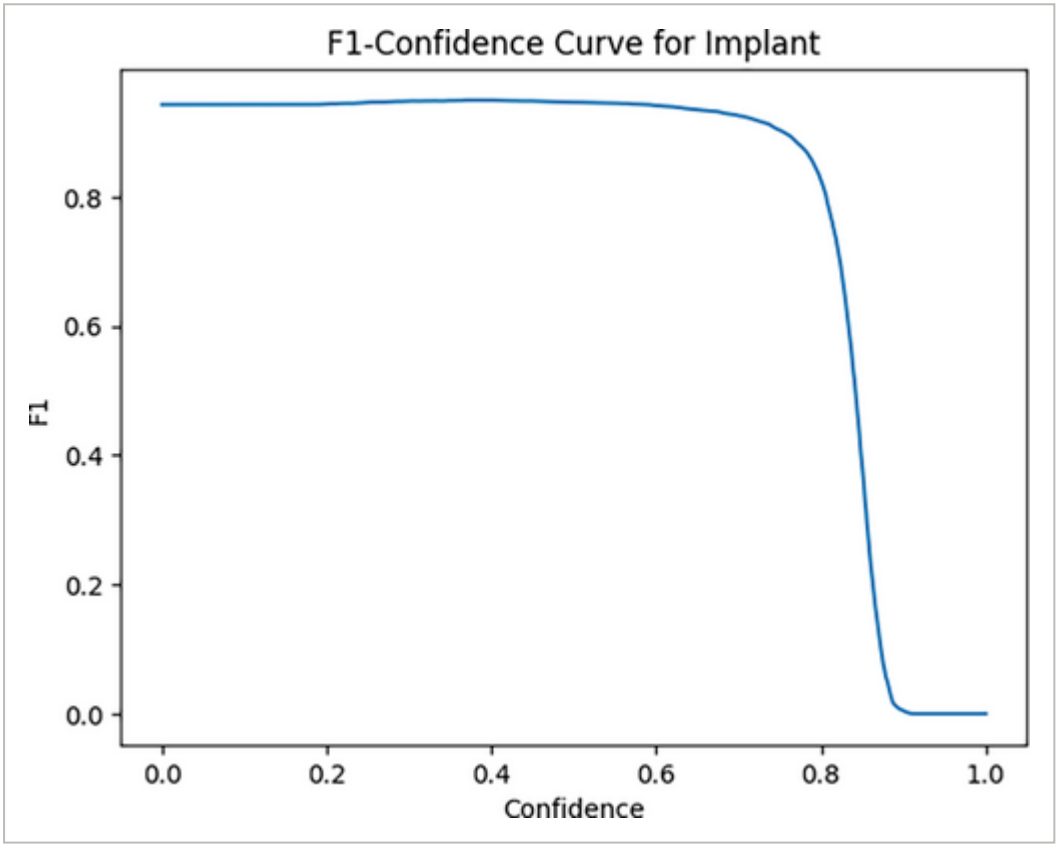

FIGURE 5

Open in figure viewer | PowerPoint

F1-Score versus confidence level.

Figure 6 depicts the relationship between precision and recall for the developed deep-learning model. The Precision-Recall curve is used to evaluate the model's performance, especially in cases of data imbalance, revealing the overall accuracy and capture rate of TP classifications. In the 0.0–0.8 recall range, the model offers high precision and recall rates, but beyond 0.8, a significant drop in precision is observed. This indicates that while the model performs optimally within a specific recall range, its accuracy decreases at higher recall levels due to an increase in FP. Thus, the model's most efficient operating range, in

Back

accurately detecting implants is essential.

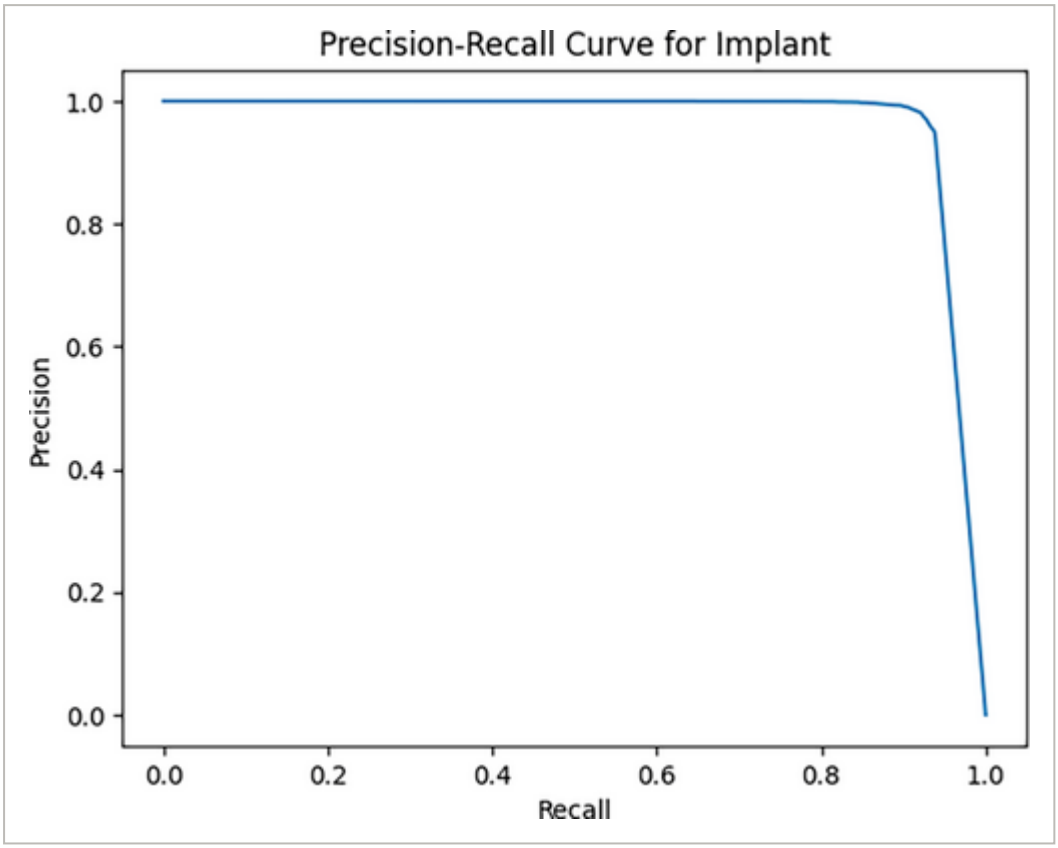

FIGURE 6

Open in figure viewer | PowerPoint

Precision-recall curve.

4 Discussion

With the advancements in AI, there has been a significant increase in the performance of deep learning models in image analysis [20-23]. In the field of medicine, many types of images such as radiological, histological, pathological, and clinical images can be analyzed using deep learning models, assisting clinicians in diagnosis and decision-making [23-25]. In this study, we aimed to detect dental implants in orthopantomographs using an AI-based approach and to number these implants.

While several AI models in the literature can detect and segment implants in orthopantomographs, the model we developed differs by not only performing detection and segmentation but also numbering the implants [15, 26-28]. The standardized structure of dental implants across different regions poses challenges for deep learning models when it comes to numbering these objects. In our model, this issue was addressed by integrating two models. In the first stage, the model performs the numbering of teeth, implants, or

distinct regions, analyzes each region in detail, and marks it as either having or not having an implant, followed by segmentation in areas with implants.

In this study, we compared the performance of various state-of-the-art models for implant numbering and segmentation, including YOLOv8, RetinaNet, Faster R-CNN, DETR, U-Net, Mask R-CNN, and DeepLab v3+ (Table S1). Among the implant-numbering models, YOLOv8 achieved the highest overall performance. YOLOv8 also exhibited excellent consistency across different classes, with its highest performance for implant number 33 (precision: 0.993, recall: 0.988, F1: 0.990) and lowest for implant number 17 (precision: 0.992, recall: 0.981, F1: 0.986). In contrast, the other models showed lower performance; for instance, Faster R-CNN achieved precision, recall, and F1 scores of 0.973, 0.953, and 0.963 at its best and 0.946, 0.939, and 0.942 at its lowest. RetinaNet followed with peak performance values of 0.953, 0.932, and 0.942 and a low of 0.876, 0.869, and 0.872. DETR's best performance yielding precision, recall, and F1 scores of 0.941, 0.933, and 0.937 and its weakest at 0.926, 0.914, and 0.920. For implant segmentation, YOLOv8 outperformed all other models with precision, recall, and F1 scores of 0.991, 0.976, and 0.992, respectively. Mask R-CNN followed with a precision of 0.943, recall of 0.950, and F1 score of 0.946, while DeepLab v3+ achieved precision, recall, and F1 scores of 0.922, 0.924, and 0.923. U-Net demonstrated the lowest performance among the segmentation models, with precision, recall, and F1 scores of 0.884, 0.879, and 0.881. These results underscore the superiority of YOLOv8, particularly for tasks requiring both high accuracy and operational efficiency. YOLOv8's advantage lies in its unified architecture for detection and segmentation, which enables faster processing and higher accuracy. This makes it particularly well-suited for clinical applications where both speed and precision are paramount. Therefore, YOLOv8 was selected as the primary model for this study, as it provides robust and reliable performance in detecting and numbering dental implants in panoramic radiographs, outperforming its counterparts by a substantial margin. Its ability to maintain robust performance across multiple classes for implant numbering and its exceptional segmentation capabilities make it the ideal choice for clinical applications in dental implantology.

Our model achieved satisfactory results in terms of precision, recall, and F1 score for detecting and numbering dental implants in orthopantomographs. For example, the precision of the implant segmentation model was 91.4%, the recall was 90.5%, and the F1 score was 93.1%. These results suggest that the model could provide reliable results in clinical applications, offering faster and more objective outcomes compared to manual evaluations.

Previous studies on tooth numbering and implant segmentation using AI have also reported high accuracy rates. Miki et al. [29] reported a 91% success rate for their tooth-numbering algorithm on cone-beam computed tomography images. Zhang et al. [30] achieved 95% accuracy in their study of tooth numbering on periapical radiographs using AI. In a study by

Back

0.977, recall = 0.992, and F1 score = 0.984. In the study by Kohlakala et al. [32], the algorithm developed for the detection of dental implants achieved a 94.0% accuracy for segmentation/detection and 71.7% accuracy for classification/recognition. Unlike these studies, our model focused on both the segmentation and numbering of dental implants. To our knowledge, there are no similar studies that focus on the numbering of dental implants, which adds a unique contribution to the literature. Accurate segmentation and numbering of implants are crucial for the development of decision support systems in dentistry.

Integrating AI systems into clinical practice could help reduce clinicians' workloads [33, 34]. Manually analyzing large datasets is time-consuming and prone to errors [35]. With our algorithm, large datasets containing orthopantomographs can be analyzed faster, minimizing potential human errors in dental implantology studies. Analyzing a radiograph in as little as 2 ms and presenting the results in table and image segment formats highlight the potential for simplifying both research and clinical practice. The integration of the proposed AI model into clinical workflows has the potential to revolutionize routine practices in dental implantology. By automating the detection and numbering of dental implants, the model can significantly reduce the time clinicians spend on manual image analysis. Current manual analyses often require several minutes per radiograph, while the proposed AI system processes each image in milliseconds. This time-saving capability, coupled with a reduction in human error, ensures standardized and objective results. Additionally, the system's compatibility with existing clinical software could facilitate seamless adoption, enabling automatic generation of detailed reports and integration with electronic health records (EHRs), thus enhancing overall efficiency and patient outcomes. At the same time, with the development and integration to be made in this model, peri-implant pathologies can be detected, evaluations can be made faster with CBCT integration, or contribution can be made to the production of implant-supported prosthesis. Current and potential uses of the model in the clinical workflow are shown in Figure 7.

Back

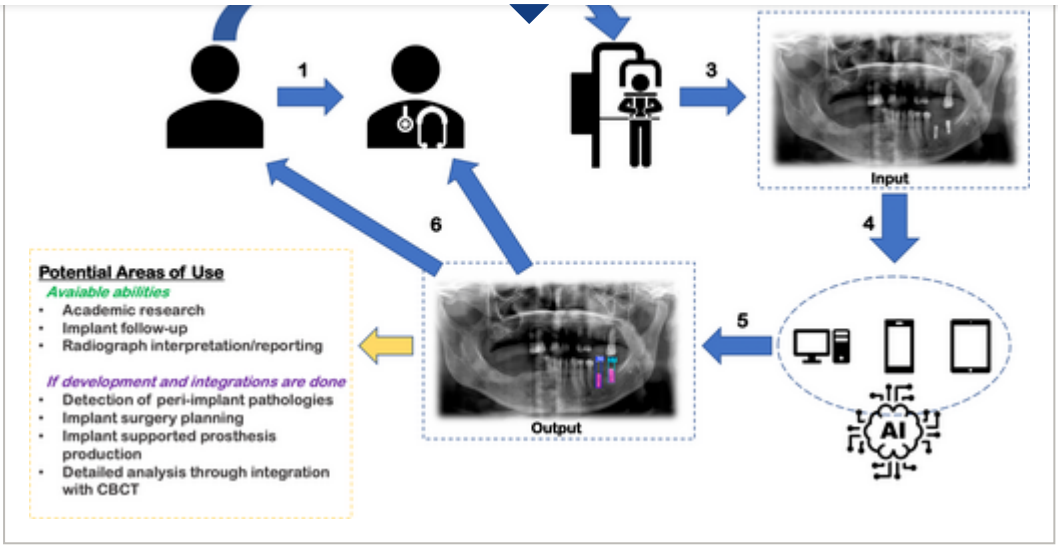

FIGURE 7

Open in figure viewer | PowerPoint

The clinical workflow diagram for the developed AI model.

While the proposed model demonstrates high accuracy in detecting and numbering dental implants, certain limitations must be addressed. First, the study utilized a dataset from a single institution, encompassing specific implant designs and brands. Expanding the dataset to include diverse implant types and imaging settings will enhance the model's generalizability. The second limitation pertains to how angled dental implants are numbered. For example, in procedures like all-on-four, where implants are placed at an angle of up to 45° [36], the coronal part of the implant might be in the premolar region while the apex lies in the canine region. Although the model was adjusted to prioritize the coronal positioning of implants during numbering, additional refinements are needed to address such scenarios more robustly. From a clinical perspective, this AI model holds significant promise. By rapidly analyzing large datasets, it reduces the workload of dental professionals, especially in high-volume practices. The model could also be employed for preoperative planning, enabling clinicians to assess implant distribution efficiently. Its potential integration with clinical decision support systems ensures consistent and objective analyses, benefiting both practitioners and patients.

In conclusion, the deep learning model developed in this study successfully detected and numbered dental implants in orthopantomographs with high accuracy, demonstrating promise as a tool for clinical applications. The use of AI-based systems in the field of dentistry not only increases the accuracy of clinical decisions but also reduces the workload of dental practitioners. Future studies will allow these technologies to be tested on a broader scale and implemented in real-world applications.

Back

Yunus Balel: concept/design, data collection/analysis, drafting article, critical revision of the article, approval of article, statistics. **Kaan Sağtaş:** concept/design, data analysis, critical revision of the article, approval of article, statistics. **Fatih Teke:** data analysis, approval of article, statistics. **Mehmet Ali Kurt:** data analysis, approval of article, statistics.

Acknowledgments

ChatGPT was used to correct the English grammar of the text. The authors checked the final version and accepted full responsibility.

Conflicts of Interest

The authors declare no conflicts of interest.

Data Availability Statement

Research data are not shared.

Supporting Information

Filename	Description
cid70000-sup-0001-Supplementary_Material-1.png PNG image, 457.5 KB	**Figure S1.** Examples of augmented images.
cid70000-sup-0002-Supplementary_Material-2.docx Word 2007 document , 24.7 KB	**Table S1.** Training performance metrics of models with different architectures.

Please note: The publisher is not responsible for the content or functionality of any supporting information supplied by the authors. Any queries (other than missing content) should be directed to the corresponding author for the article.

References

1 B. Molander, “Panoramic Radiography in Dental Diagnostics,” *Swedish Dental Journal* **119** (1996): 1–26.

Back

2 S. Yilmaz, M. Tasyurek, M. Amuk, M. Celik, and E. M. Canger, "Developing Deep Learning Methods for Classification of Teeth in Dental Panoramic Radiography," *Oral Surgery, Oral Medicine, Oral Pathology, Oral Radiology* **138** (2024): 118–127, https://doi.org/10.1016/j.oooo.2023.02.021.

PubMed | Web of Science® | Google Scholar

3 S. AlQarni, G. Chandrashekar, E. E. Bumann, and Y. Lee, "Incremental Learning for Panoramic Radiograph Segmentation," In *Annual International Conference of the IEEE Engineering in Medicine & Biology*, (2022), 557–561, https://doi.org/10.1109/EMBC48229.2022.9871995.

Google Scholar

4 J. H. Kamdar, J. Jeba Praba, and J. J. Georrge, " Artificial Intelligence in Medical Diagnosis: Methods, Algorithms and Applications," in *Machine Learning With Health Care Perspective: Machine Learning and Healthcare* (Cham: Springer International Publishing, 2020), 27–37.

Google Scholar

5 S. H. Park and K. Han, "Methodologic Guide for Evaluating Clinical Performance and Effect of Artificial Intelligence Technology for Medical Diagnosis and Prediction," *Radiology* **286** (2018): 800–809.

PubMed | Web of Science® | Google Scholar

6 R. Najjar, "Redefining Radiology: A Review of Artificial Intelligence Integration in Medical Imaging," *Diagnostics* **13** (2023): 2760.

PubMed | Web of Science® | Google Scholar

7 D. Jin, A. P. Harrison, L. Zhang, et al., " Artificial Intelligence in Radiology," in *Artificial Intelligence in Medicine* (Amsterdam, The Netherlands: Elsevier, 2021), 265–289.

Google Scholar

8 A. Hosny, C. Parmar, J. Quackenbush, L. H. Schwartz, and H. J. W. L. Aerts, "Artificial Intelligence in Radiology," *Nature Reviews Cancer* **18** (2018): 500–510.

Back

9 J. Liu, Y. Liu, S. Li, S. Ying, L. Zheng, and Z. Zhao, "Artificial Intelligence-Aided Detection of Ectopic Eruption of Maxillary First Molars Based on Panoramic Radiographs," *Journal of Dentistry* **125** (2022): 104239.

PubMed | Web of Science® | Google Scholar

10 S. Vishwanathaiah, H. N. Fageeh, S. B. Khanagar, and P. C. Maganur, "Artificial Intelligence Its Uses and Application in Pediatric Dentistry: A Review," *Biomedicine* **11** (2023): 788.

Google Scholar

11 M. E. Celik, "Deep Learning Based Detection Tool for Impacted Mandibular Third Molar Teeth," *Diagnostics* **12** (2022): 942, https://doi.org/10.3390/diagnostics12040942.

PubMed | Web of Science® | Google Scholar

12 E. D. Costa, H. Gaêta-Araujo, J. A. Carneiro, et al., "Development of a Dental Digital Data Set for Research in Artificial Intelligence: The Importance of Labeling Performed by Radiologists," *Oral Surgery, Oral Medicine, Oral Pathology, Oral Radiology* **138** (2024): 205–213.

PubMed | Web of Science® | Google Scholar

13 M. Paredes, "Can Artificial Intelligence Help Reduce Human Medical Errors? Two Examples From ICUs in the US and Peru," 2021 Techpolicy Institute.

Google Scholar

14 B. K. Baurasien, H. S. Alareefi, D. B. Almutairi, et al., "Medical Errors and Patient Safety: Strategies for Reducing Errors Using Artificial Intelligence," *International Journal of Health Sciences* **7** (2023): 3471–3487.

Google Scholar

15 D.-W. Lee, S.-Y. Kim, S.-N. Jeong, and J.-H. Lee, "Artificial Intelligence in Fractured Dental Implant Detection and Classification: Evaluation Using Dataset From Two Dental Hospitals," *Diagnostics* **11** (2021): 233.

Back

16 A. Y. Alqutaibi, R. S. Algabri, D. Elawady, and W. I. Ibrahim, "Advancements in Artificial Intelligence Algorithms for Dental Implant Identification: A Systematic Review With Meta-Analysis," *Journal of Prosthetic Dentistry* (2023).

Google Scholar

17 B. Wang, "A Parallel Implementation of Computing Mean Average Precision," ArXiv Prepr ArXiv220609504, (2022).

Google Scholar

18 A. N. Gajjar and J. Jethva, "Intersection Over Union Based Analysis of Image Detection/Segmentation Using CNN Model," In *2022 Second International Conference on Power, Control and Computing Technologies*, IEEE, (2022), 1–6.

Google Scholar

19 E. Yazan and M. F. Talu, "Comparison of the Stochastic Gradient Descent Based Optimization Techniques," In *2017 International Artificial Intelligence and Data Processing Symposium*, IEEE, (2017), 1–5.

Google Scholar

20 J. Ker, L. Wang, J. Rao, and T. Lim, "Deep Learning Applications in Medical Image Analysis," *IEEE Access* **6** (2017): 9375–9389.

Web of Science® | Google Scholar

21 M. Puttagunta and S. Ravi, "Medical Image Analysis Based on Deep Learning Approach," *Multimedia Tools and Applications* **80** (2021): 24365–24398.

PubMed | Web of Science® | Google Scholar

22 G. Litjens, T. Kooi, B. E. Bejnordi, et al., "A Survey on Deep Learning in Medical Image Analysis," *Medical Image Analysis* **42** (2017): 60–88.

PubMed | Web of Science® | Google Scholar

Back

PubMed | Web of Science® | Google Scholar

24 A. S. Sultan, M. A. Elgharib, T. Tavares, M. Jessri, and J. R. Basile, "The Use of Artificial Intelligence, Machine Learning and Deep Learning in Oncologic Histopathology," *Journal of Oral Pathology & Medicine* **49** (2020): 849–856.

PubMed | Web of Science® | Google Scholar

25 J. Van der Laak, G. Litjens, and F. Ciompi, "Deep Learning in Histopathology: The Path to the Clinic," *Nature Medicine* **27** (2021): 775–784.

CAS | PubMed | Web of Science® | Google Scholar

26 N. Adnan, W. Bin Khalid, and F. Umer, "An Artificial Intelligence Model for Instance Segmentation and Tooth Numbering on Orthopantomograms," *International Journal of Computerized Dentistry* **26** (2023): 301.

PubMed | Web of Science® | Google Scholar

27 S. Gülüm, S. Kutal, K. Cesur Aydin, G. Akgün, and A. Akdağ, "Effect of Data Size on Tooth Numbering Performance via Artificial Intelligence Using Panoramic Radiographs," *Oral Radiology* **39** (2023): 715–721.

PubMed | Web of Science® | Google Scholar

28 R. P. da Mata Santos, H. E. Vieira Oliveira Prado, I. S. Aranha Neto, et al., "Automated Identification of Dental Implants Using Artificial Intelligence," *International Journal of Oral and Maxillofacial Implants* **36** (2021): 36–923.

Google Scholar

29 Y. Miki, C. Muramatsu, T. Hayashi, et al., "Classification of Teeth in Cone-Beam CT Using Deep Convolutional Neural Network," *Computers in Biology and Medicine* **80** (2017): 24–29, https://doi.org/10.1016/j.compbiomed.2016.11.003.

PubMed | Web of Science® | Google Scholar

Back

s://doi.org/10.1016/j.compmedimag.2018.07.001.

PubMed | Web of Science® | Google Scholar

31 W. S. Jang, S. Kim, P. S. Yun, et al., "Accurate Detection for Dental Implant and Peri-Implant Tissue by Transfer Learning of Faster R-CNN: A Diagnostic Accuracy Study," *BMC Oral Health* **22** (2022): 591, https://doi.org/10.1186/s12903-022-02539-x.

PubMed | Web of Science® | Google Scholar

32 A. Kohlakala, J. Coetzer, J. Bertels, and D. Vandermeulen, "Deep Learning-Based Dental Implant Recognition Using Synthetic X-Ray Images," *Medical & Biological Engineering & Computing* **60** (2022): 2951–2968, https://doi.org/10.1007/s11517-022-02642-9.

PubMed | Web of Science® | Google Scholar

33 W.-J. Tong, S.-H. Wu, M.-Q. Cheng, et al., "Integration of Artificial Intelligence Decision Aids to Reduce Workload and Enhance Efficiency in Thyroid Nodule Management," *JAMA Network Open* **6** (2023): e2313674.

PubMed | Web of Science® | Google Scholar

34 A. Boonstra and M. Laven, "Influence of Artificial Intelligence on the Work Design of Emergency Department Clinicians a Systematic Literature Review," *BMC Health Services Research* **22** (2022): 669.

PubMed | Web of Science® | Google Scholar

35 S. C. Lewis, R. Zamith, and A. Hermida, "Content Analysis in an Era of Big Data: A Hybrid Approach to Computational and Manual Methods," *Journal of Broadcasting & Electronic Media* **57** (2013): 34–52.

Web of Science® | Google Scholar

36 T. Begg, G. A. V. M. Geerts, and J. Gryzagoridis, "Stress Patterns Around Distal Angled Implants in the All-On-Four Concept Configuration," *International Journal of Oral and Maxillofacial Implants* **24** (2009): 663–671.

PubMed | Web of Science® | Google Scholar

Back

Citing Literature

Download PDF

ABOUT WILEY ONLINE LIBRARY

Privacy Policy
Terms of Use
About Cookies
Manage Cookies
Accessibility
Wiley Research DE&I Statement and Publishing Policies

HELP & SUPPORT

Contact Us
Training and Support